

DETERMINATION OF QUATERNARY STRUCTURE BY SMALL ANGLE NEUTRON SCATTERING

*9054

D. M. Engelman and P. B. Moore

Department of Molecular Biophysics and Biochemistry,
Yale University, New Haven, Connecticut 06520

1 PREFACE

In the past few years investigators have begun to use small angle neutron scattering as a method for studying the structure of biological materials in solution. This area is in its infancy; only a handful of experimental results have appeared in the literature. Accordingly, a survey of the field at this point must be considered a preview rather than a review. Thus the objective of this article is to familiarize the reader with the background of this field so he will understand the interest in it, and be able to judge what studies of this kind might contribute to his own progress. It will be the task of others at some future date to judge whether these techniques have fulfilled their promise.

2 INTRODUCTION

Neutrons, like all small particles, display wave properties. The wavelength of a neutron, λ , is related to its momentum, p , according to de Broglie's equation, $\lambda = h/p$, where h is Planck's constant. Using the de Broglie relationship it can be readily shown that neutrons having the same kinetic energies as gas molecules at room temperature, that is, thermal neutrons, have wavelengths of about an angstrom (10^{-8} cm). Thus, beams of thermal neutrons can be used to conduct diffraction experiments that give information about the structure of matter at atomic resolution. In fact it is possible to perform neutron scattering experiments on biological materials analogous to the X-ray scattering experiments that have been the mainstay of structural biochemists for many years.

In this article we emphasize the application of neutron scattering to the study of the spatial organization of subunits in macromolecular aggregates. [A more general review of biological applications of neutron scattering can be found in Volume 1 of this series (1). For other reviews see (2, 3).] This field of research is the

product of a marriage between the small angle solution-scattering methodology worked out over the last fifty years by investigators using X rays and the newer area of neutron scattering. The merger has been brought about by the recognition that neutron radiation offers substantial advantages over X radiation for the study of macromolecular structure by small angle methods.

In order to understand what these advantages are we must first consider how neutrons interact with matter. We go on to discuss the aspects of small angle theory relevant to the study of macromolecular aggregates. We then show what might be done by the neutron technique and discuss the results available in the literature.

3 THE INTERACTION OF THERMAL NEUTRONS WITH MATTER

There are three possible outcomes of an encounter between a neutron and an atom: 1. absorption of the neutron, 2. scattering of the neutron, 3. no interaction. [For general information on neutron scattering see (4, 5).] Absorption of the neutron results in the addition of the neutron to the nucleus of the absorbing atom generating thereby a new nuclide. Scattering of the neutron produces a change in the direction or speed of flight (or both) of the neutron. If there is no interaction, the neutron proceeds in its original direction of flight with unaltered speed.

Scattering events are classified as elastic or inelastic depending on whether or not the scattering process conserves the kinetic energy of the neutron. It is elastic events that concern us here because they produce the neutron interference effects that give information about molecular structure. Inelastic scattering appears to be quantitatively less important than elastic scattering in solutions of macromolecules.

3.1 *Elastic Scattering*

Scattering events involving the atomic species common in biological systems are dominated by neutron-nucleus interactions (6). Both the nucleus of an atom and the range of the forces involved in neutron-nucleus interactions are orders of magnitude smaller than the wavelength of a thermal neutron. Therefore an incident thermal neutron sees an atom as a point scatterer. The probability of the neutron being scattered in a given direction is equal in all directions. Thus if the incident neutron is represented as a wave of amplitude 1.0 and wavelength λ , the scattered wave, ψ_s , will have the form

$$\psi_s = -(b/r) \exp(2\pi ir/\lambda), \quad 1.$$

where r is the distance from the scattering nucleus to the observer. The coefficient b in equation 1 is called the "scattering length." Its magnitude is a measure of the probability of the scattering event. The scattered wave has a negative sign because it is usually 180° out of phase relative to the incident wave.

The scattering length of an atom depends on its nuclear mass, spin, and energy levels. Atoms with nuclear spin in fact have two scattering lengths, often quite different: one for an encounter with a neutron whose spin is up and another

for a spin down encounter. Furthermore, the scattering lengths of different isotopes of the same element differ. Thus when a sample of an element is allowed to scatter neutrons, part of the scattering will reflect random variations in sample scattering length due to the random distribution of nuclear spin orientations and isotopic species. This random component is called "incoherent elastic scattering," and is spatially isotropic. There will also be a component whose spatial distribution reflects the spatial distribution of atoms in the sample. This correlated component is called "coherent elastic scattering." Only coherent scattering events produce interference. It is upon these that structural analysis depends.

3.2 Cross Sections

The scattering properties of virtually all elements and of many pure isotopes have been measured and the results tabulated in the literature (7). Table 1 gives the neutron scattering parameters for the nuclei of most interest in biology. The scattering length for each species, b , its coherent elastic cross section, σ_c ($\sigma_c = 4\pi b^2$), its total elastic cross section, σ_t , and its absorption cross section, σ_a , are listed. The incoherent elastic cross section of each atomic species is simply $(\sigma_t - \sigma_c)$. Cross sections are used to calculate the absolute frequency of scattering or absorption events. If an atom of scattering length, b , is placed in a neutron beam having a flux of N neutrons per unit area per unit time, $N\sigma_c$ neutrons per unit time will be scattered coherently through the surface of a sphere unit radius. There will be Nb^2 neutrons scattered per steradian.

Three important facts emerge from Table 1. First, there is an enormous difference in scattering length between hydrogen and deuterium. The negative sign given to the scattering length of H implies that neutrons scattered by H undergo no phase retardation relative to the incident wave, instead of the usual 180° shift. Thus when a hydrogen-containing structure is analyzed by neutron

Table 1 Neutron scattering parameters for biological atoms^a

Species/Parameter	b	σ_c	σ_t	σ_a
H	-0.374	1.76	81.5	0.19
D	+0.667	5.59	7.6	0.0005
C	+0.665	5.56	5.6	0.003
N	+0.940	11.10	11.14	1.1
O	+0.580	4.23	4.24	0.0001
P	+0.51	3.27	3.6	0.09
S	+0.285	1.02	1.2	0.28

^a Coherent elastic scattering lengths, b , are given in Fermis ($1\text{F} = 10^{-12}$ cm). The values listed are from the 1972 compilation of scattering data by C. G. Shull, as quoted in (1). The units for σ_c , σ_t , and σ_a are barns ($1 \text{ barn} = 10^{-24}$ cm²). Coherent elastic cross sections were calculated from b values; $\sigma_c = 4\pi b^2$. Total cross sections, σ_t , and absorption cross sections, σ_a , were obtained from (7).

crystallography, hydrogen atoms will appear in the final map of the structure as regions of negative density, while all atoms with positive scattering lengths are represented as positive density. Second, the scattering lengths of the atoms in Table 1 (except H) are of roughly the same magnitude and show no obvious change as a function of atomic number. In contrast, scattering lengths of atoms for X rays are proportional to the number of electrons they contain and hence atomic number. In X-ray scattering experiments atoms with many electrons are readily detected and hydrogen with its single electron is virtually ignored. The contribution of hydrogen to the neutron scattering of a molecule is substantial by comparison. Thus a primary application of neutron scattering in crystallography has been determination of hydrogen atom positions, e.g. (8). Third, the incoherent elastic scattering cross sections are small compared with the coherent cross sections for all atoms of biological interest except hydrogen.

Incoherently scattered neutrons do not contribute to interference effects and hence provide no structural information about a specimen. They are distributed in space isotropically, contributing a uniform background to the scattered signal. Because the detectors used in ordinary scattering experiments accept radiation over a small solid angle (10^{-4} – 10^{-5} sr), the background produced by a sample with a large incoherent cross section is modest. A more important effect of incoherence is simply the loss of neutrons available for coherent scattering. A 2.0 mm thick specimen of H_2O reduces the intensity of a neutron beam passing through it by about 67%. In order to avoid such losses in biological specimens, one avoids hydrogen. The usual trick is to use D_2O instead of H_2O as the specimen solvent. It should be pointed out, however, that measurements can be made in H_2O solvents provided reasonably thin specimens can be prepared. In some cases valuable data may be obtained from such measurements; incoherence is not a reason for categorically excluding them from consideration.

3.3 Scattering Density, The Small Angle Approximation

The distribution in space of the radiation (coherently) scattered by an isolated object is related to the Fourier transform of the distribution of scattering length within the object (9). If we have an object whose three-dimensional distribution of scattering length is given by $\rho(\mathbf{r})$, then its Fourier transform, $F(\mathbf{R})$, will be given by

$$F(\mathbf{R}) = \int_V \rho(\mathbf{r}) \exp(2\pi i \mathbf{r} \cdot \mathbf{R}) dV, \quad 2.$$

the integral being taken over the region of space, V , which is occupied by the object. The vector \mathbf{R} points in the direction given by the difference between a unit vector in the direction from the scattering object to the observer and a unit vector in the direction of the incident radiation. The magnitude of \mathbf{R} is $(2 \sin \theta/\lambda)$ where θ is half the scattering angle and λ is the wavelength of the incident radiation. The scattering angle, 2θ , is simply the angle between the beam that passes directly through the specimen and the scattered beam. The intensity of radiation measured by a detector at some orientation relative to the incident beam due to the scattering of the object is proportional to $|F(\mathbf{R})|^2$.

The small angle portion of a scattering profile is generally taken as extending from

$2\theta = 0^\circ$ to $2\theta = 5^\circ$. Using Bragg's law, assuming a radiation wavelength of 1–10 Å, it can be shown that the atom-to-atom variations in scattering length within a molecule do not contribute to scattering at these angles. In the low angle scattering region, it is valid to think of a macromolecule as an assembly of one or a few large units, each of which has a shape and an average scattering length per unit volume, or "scattering density," ρ ,

$$\rho = (1/V) \sum b_i, \quad 3.$$

where V is the volume of the molecule; the summation of scattering lengths, b_i , runs over all its atoms. For a small, chemically homogeneous macromolecule, the low angle scattering profile is proportional to the product of its scattering density, ρ , times the Fourier transform of its shape, squared.

So far we have been implicitly assuming that the molecule whose scattering is being considered is in a vacuum. A macromolecular specimen, however, ordinarily includes a solvent. It is easy to show that the correct way to account for the solvent in a low angle scattering experiment is to substitute $(\rho - \rho_{\text{sol}})$ in all expressions in place of ρ . Thus in the small angle approximation we have

$$|F(\mathbf{R})|^2 = (\rho - \rho_{\text{sol}})^2 \left[\int_{-\infty}^{+\infty} f(\mathbf{r}) \exp(2\pi i \mathbf{R} \cdot \mathbf{r}) dV \right]^2, \quad 4.$$

where $f(\mathbf{r})$ is a function that has a value of zero at all points except those within the boundary of the molecule where its value is 1.0. $(\rho - \rho_{\text{sol}})$ will be called the "contrast" between the solvent and the molecule in question.

It should be remembered when making scattering density calculations using equation 3 that macromolecules contain exchangeable hydrogens (43). For this reason scattering densities are dependent on solvent deuteration. Thus to make an accurate estimate of the scattering density of a macromolecule in any situation, the fraction of its hydrogen component exchanged with solvent must be known.

3.4 Scattering Densities of Biological Materials

Table 2 gives approximate scattering densities for a number of biologically important materials. The densities of these substances differ greatly (Table 2A) and can be varied over a remarkably large range by substitution of D for H (Table 2A vs 2B). Furthermore, the scattering density of D_2O is above and that of H_2O below that of all fully H-substituted macromolecules.

We know from equation 4 that a molecule will give no small angle scattering if its scattering density equals that of its solvent. Since we can mix D_2O and H_2O in any proportion we wish, it is clearly possible to match the solvent to the scattering density of any H-substituted macromolecule. This maneuver is called "contrast matching" and is the tool that makes quaternary structure analysis by neutron scattering possible.

Suppose we wish to examine an object consisting of two parts differing in scattering density. To study one part independently, all we have to do is contrast match the other. It will then "disappear" from the experiment as far as low angle scattering is concerned and only the scattering of the unmatched portion will be seen. This

Table 2 Neutron and X-ray scattering densities for substances of biological importance^a

Substance	ρ	
	Neutron	X ray
A. Fully H-substituted		
i. H ₂ O	-0.55	+9.3
ii. Protein	+3.11	+12.4
iii. Nucleic acid	+4.44	+16.0
iv. Fatty acid	-0.01	+8.2
v. Carbohydrate	+4.27	+14.1
B. Fully D-substituted		
i. D ₂ O	+6.36	+9.3
ii. Protein	+8.54	+12.4
iii. Nucleic acid	+7.44	+16.0
iv. Fatty acid	+6.89	+8.2
v. Carbohydrate	+8.07	+14.1

^aAll scattering densities are in units of 10^{-14} cm/Å³. Neutron calculations were done assuming all exchangeable hydrogens in all cases are fully D-substituted, employing equation 3. 50S ribosomal protein and 23S RNA, both from *E. coli*, were taken as examples of nucleic acid and protein (50). The fatty acid used for computing (iv) was stearic acid and the carbohydrate (v) was glucose.

type of experiment can be done on lipoproteins or nucleoproteins, for example, where internal scattering density differences occur naturally over large regions of the structure. It can be extended to the study of structures normally lacking internal scattering density differences provided means can be found for selectively substituting D for H in specific regions. Since the manipulations required to carry out such experiments involve only isotopic changes, the perturbations caused in the structures being studied are minimal.

X-ray scattering density is proportional to electron density (10). Different kinds of macromolecules differ in electron density just as they differ in neutron scattering density (Table 2). These differences can be used in small angle experiments. The range of possibilities, however, is limited for X rays. Solvent electron density can be raised by addition of solutes of high electron density; however, the range of electron densities that can be reached in water solution includes that of bulk protein, but not that of bulk nucleic acid. The choice of electron dense solute is limited by the solubility of the solute employed and by the stability of the structures under investigation. Large scale manipulation of the X-ray scattering density of a macromolecule is virtually impossible because it requires one to add (or subtract) electrons for the structure, which can only be done by massive chemical modification.

In order to produce alterations in protein X-ray scattering density comparable to the scattering density changes achieved in a neutron experiment by going from all H to all D, one would have to label every other residue with Hg. It is unlikely that the derivative molecule would be isomorphous with the native structure even if the synthesis could be accomplished. Thus, it is clear that contrast manipulation is a far more powerful tool for neutron small angle work than it is for X rays.

4 QUATERNARY STRUCTURE ANALYSIS

4.1 *General Concepts*

Everything said so far about small angle scattering is true regardless of the state of the material being examined. Since our interest is in the analysis of structures available only in noncrystalline form, e.g. in solution, we should consider the implications of this constraint. [For general discussions of solution scattering, see (9–12).]

If the scattering profile of an isolated macromolecule is $|F(\mathbf{R})|^2$, then the macromolecular contribution to the scattering of a dilute solution of such molecules will be proportional to the spherically averaged profile, $\overline{|F(\mathbf{R})|^2}$. Because of its rotationally averaged nature, such a profile gives information about the relative importance of density fluctuations of different periodicities, $|\mathbf{R}|^{-1}$, but says nothing about the directional distribution of these fluctuations in the molecule or their relative phases. Clearly three-dimensional atomic coordinates for a macromolecule cannot be derived from such data. In fact, only molecules as simple as diatomic gases can be fully characterized from a single solution-scattering measurement. Thus, to determine the location of subunits in a macromolecular aggregate by solution scattering the overall problem must be simplified. One approach is to reduce it to a series of measurements of distances between pairs of subunits (or regions) within the aggregate, each such measurement being conceptually analogous to determining the interatomic distance in a diatomic gas. The quaternary structure of the whole aggregate follows from these distances by triangulation.

4.2 *Interpretation of Small Angle Data*

Assuming our experimental technique is adequate to provide a good estimate of $\overline{|F(\mathbf{R})|^2}$ (see below), the next issue is to interpret this profile in terms of the molecule's structure. A key contribution in the theory of the interpretation of such profiles was made by Guinier in 1939 (13). He demonstrated that at scattering angles close to zero, the scattering profile of all molecules, $I(R)$, is a Gaussian:

$$I(R) = I(O) \exp(-4\pi R^2 R_g^2/3). \quad 5.$$

$I(O)$ in this expression is the forward scatter, that is, the scatter given by the specimen in the direction of the incident beam. R_g is called the molecule's "radius of gyration." For a solution-scattering experiment we have

$$R_g^2 = \frac{\int_v [\rho(\mathbf{r}) - \rho_{\text{sol}}] |\mathbf{r}|^2 dV}{\int_v [\rho(\mathbf{r}) - \rho_{\text{sol}}] dV}. \quad 6.$$

R_g gets its name by analogy with the mechanical concept defined by substituting mass density for scattering density in equation 6. Note that in a neutron experiment, R_g^2 can be zero or negative, in contrast to the mechanical quantity, which is always positive.

Equation 5, known as the Guinier approximation, describes the scattering profile of any molecule at scattering angles close to 0. The range of angles over which it holds depends on the shape of the molecule being examined (14). It happens that for macromolecules of moderate axial ratio, the range of angles over which the approximation holds is accessible experimentally. Thus small angle data give radius of gyration estimates for most molecules. There are parameters related to the radius of gyration that can be obtained for objects with extreme axial ratios (12, 14).

The form of the scattering curve outside the Guinier region is generally interpreted as giving information about molecular shape (14). This interpretation must be regarded with caution because at higher angles the contribution of internal fluctuations in scattering length to the profile becomes increasingly important. Stuhmann and his co-workers (15–17) have recently analyzed the relative contributions of shape [i.e. $f(\mathbf{r})$ in equation 4] and internal density variations to $[F(\mathbf{R})]^2$ for macromolecules. They have shown that the X-ray solution-scattering profile of a molecule may be experimentally resolved into its shape and internal fluctuation components (17). Since the technique employed relies on contrast manipulation it lends itself ideally to neutron methods (18).

To analyze the quaternary structure of a macromolecular aggregate by small angle techniques, the experiment is arranged so that internal variations in scattering density can be detected in the small angle pattern. Two strategies employing this general philosophy have been proposed. In both approaches the idea is to simplify analysis by manipulating contrasts in a macromolecular aggregate to make the contributions from just two subunits dominate the scattering profile. In theory the three-dimensional arrangement of n subunits in a complex aggregate can be obtained from a series of $4n - 10$ pairwise measurements.

4.3 Radius of Gyration Analysis

Suppose for simplicity that an aggregate is being studied that consists of one copy of subunit α and one copy of subunit β . Suppose also that α and β can be studied independently in native conformation. Since the aggregate is composed of α and β , from the parallel axis theorem in mechanics a simple relationship can be deduced relating the three radii of gyration, $R_{\alpha\beta}$, R_α , and R_β (19):

$$R_{\alpha\beta}^2 = f_\alpha R_\alpha^2 + f_\beta R_\beta^2 + f_\alpha f_\beta \Delta_{\alpha\beta}^2. \quad 7.$$

In Equation 7 $\Delta_{\alpha\beta}$ is the separation between the centers of mass of subunits α and β in the aggregate. If the total scattering length of $\alpha\beta$ is 1.0, f_α is the portion contributed by α and f_β is the portion contributed by β . Thus a measurement of the three radii of gyration can lead to an estimate of $\Delta_{\alpha\beta}$, the separation between subunits.

Experiments of this design have been attempted by X-ray techniques, e.g. (20).

Their weakness is that the estimates of $\Delta_{\alpha\beta}$ obtained depend on the assumption that R_α and R_β are the same for the isolated subunits and the subunits in the aggregate, an assumption impossible to verify by X-ray methods. A better experiment can be done using neutrons. Suppose we make α and β different in degree of deuteration so that $\rho_\alpha \neq \rho_\beta$. Then what we can do is form $\alpha\beta$ and measure its radius of gyration in a solvent chosen first so that $\rho_{\text{sol}} = \rho_\beta$ and then so that $\rho_{\text{sol}} = \rho_\alpha$. In this way R_α and R_β will be found in situ in the aggregate. Then $R_{\alpha\beta}$ is measured under subunit labeling and solvent calculations such that $\rho_\alpha = \rho_\beta$ and $\Delta_{\alpha\beta}$ is obtained.

If an experiment can be done by contrast manipulation on a two subunit structure, in principle it can be done on structures with many different subunits. In this way all the intersubunit distances (Δ_{ij}) can be obtained. These distances refer to separations between subunit centers of scattering mass. The values obtained are in principle independent of the shape and relative orientation of the subunits. Given a set of such distances, the three-dimensional locations of the centers of mass of the subunits may be specified by triangulation with only the handedness of the arrangement indeterminate (21, 22). In the framework of the current discussion, such a map would constitute a full description of the quaternary structure of a macromolecular aggregate. The limitation on the complexity of the structure one can approach by radius of gyration analysis is set by the size of the subunits relative to the whole structure and the precision with which the density matching can be done. Close density matching is not required for analysis of a two-subunit structure, but is virtually essential for more complex aggregates.

4.4 Interference Analysis

Suppose that by contrast manipulation we can generate a multisubunit aggregate where two components contrast with the rest of the structure that in turn is contrast matched with the solvent (21, 22). Provided the subunits have spherical symmetry, the scattering of this specimen, $I(R)$, will be given by the Debye expression (23),

$$I(R) = \alpha \sum_{i=1}^2 \sum_{j=1}^2 F_i(R)F_j(R) \frac{\sin 2\pi R\Delta_{ij}}{2\pi R\Delta_{ij}}, \quad 8.$$

where $F_i(R)$ is the Fourier transform of the scattering density distribution of the i th subunit. If we expand equation 8, making appropriate allowance for solvent scattering density and the usual small angle approximation, and omitting some proportionality constants, we obtain

$$I(R) = I_1(R) + I_2(R) + 2(\rho - \rho_{\text{sol}})^2 F_1(R)F_2(R) \frac{\sin 2\pi R\Delta_{12}}{2\pi R\Delta_{12}} \quad 9.$$

where $I_1(R)$, $I_2(R)$, $F_1(R)$, and $F_2(R)$ are the scattering profiles and Fourier transforms of subunits 1 and 2. If we also make a sample that has only subunit 1 contrasted and measure its profile and do the corresponding experiment for subunit 2, we can measure $I_1(R)$ and $I_2(R)$. By subtracting $I_1(R)$ and $I_2(R)$ from $I(R)$ we can then isolate the $\sin x/x$ contribution from the original profile. This term represents interference produced because the two strongly scattering subunits

are held in a fixed relationship in the structure. It has a value of zero every $(2\Delta_{12})^{-1}$ in the scattering profile, where Δ_{12} is the distance between the centers of mass of subunits 1 and 2. Thus the intersubunit spacing can be derived by inspection of $[I(R) - I_1(R) - I_2(R)]$. In order to do this subtraction experimentally, the profiles for the three specimens must be obtained under strictly comparable conditions.

The interference term has the form given in equation 9 only for subunits with spherical symmetry. Its property of crossing zero at regular intervals related to the distance between centers of mass is, however, insensitive to variations in subunit shape and relative orientation (Moore & Engelman, unpublished results).

Moreover, the condition that the background portion of the structure be matched to the solvent, which makes the system simpler to think about, is not a requirement for making the measurement. If matching is not done, all that is necessary is that one also measure the profile of the structure with no internally contrasting subunits, $I_N(R)$. The interference term, $X(R)$, is then given by

$$X(R) = [I(R) + I_N(R)] - [I_1(R) + I_2(R)].$$

Because perfect density matching is not a requirement of this approach, it should be possible to apply it to structures larger than those one can examine by the radius of gyration method. In principle, if not always in practice, both radius of gyration and interference analysis can be done on the same data. The first exploits only the Guinier region; the second employs a more extended data set. Consistent answers should emerge from both.

The potentialities of interference analysis of large structures by X-ray solution scattering have been considered in the past, e.g. (24). The X-ray analogue of this experiment involves labeling specific parts of subunits in a large structure with heavy atoms and then measuring the distance between heavy atoms from the interference ripple they produce in a solution-scattering profile, as developed above. Hoppe (21) has recently explored the possibility of using this approach for large macromolecular aggregates. His calculations show that the signal-to-noise ratio in such an experiment would make it extremely difficult to do. He has also suggested an improved general strategy for making these measurements, which keeps interaggregate interference effects from obscuring the intraaggregate signal sought (21, 25). The feasibility of the X-ray approach for moderate sized molecules has been shown (21).

The neutron version of this experiment has two obvious advantages over its X-ray analogue. First, the magnitude of scattering density change obtainable by H/D ratio manipulation far outweighs anything possible by heavy atom labeling. Thus the interference signal can be made larger than in the X-ray case. Second, it is far easier to contrast match the unlabeled portions of the structure for neutron scattering than for X rays. Contrast matching increases the signal-to-noise ratio in experiments of this kind, an important point considering the small magnitude of the signal expected in complex structures.

4.5 *The Analysis of Structures with Point-Group Symmetry*

Many multisubunit aggregates of biological structures have point-group symmetry (e.g. most multienzyme complexes). Because of the presence of multiple copies of

each kind of subunit in these structures, data about separations of centers of mass between different species of subunits in the structure as a whole may be of little interest. Structures of this type have scattering profiles that are often like microcrystals on account of their high internal order. Their solution-scattering profiles often show distinct rings of intensity resembling a powder diagram, e.g. (26). The contrast manipulation approach can be usefully applied to the interpretation of these patterns. By matching, one can independently obtain scattering curves for each species of subunit in the aggregate to assess its distribution in the whole particle.

4.6 *Biochemical Considerations*

To obtain quaternary structure information about an aggregate by the neutron low angle techniques described, there must be scattering density differences in the structure one wishes to examine. These differences can be naturally occurring, that is, exist in the structures as usually prepared. However, for full elucidation of the quaternary structure of most aggregates one will have to make use of artificially produced differences in scattering density. The obvious way to produce such differences is to selectively deuterate different parts of the structure. Controlled deuteration is possible for those structures that can be dissociated into their subunits and then reconstituted. Microorganisms such as *E. coli* tolerate D in their growth media at levels approaching 100%. By adjusting growth conditions one can obtain macromolecular aggregates (and hence their subunits) at whatever level of deuteration is required. Thus for those bacterial multisubunit aggregates that can be reconstituted, determination of subunit positions by neutron scattering is a real possibility.

As experimental technique improves, it may become possible to exploit small scattering density differences for quaternary structure investigations. In this event, it will be possible to extend the range of accessible structures to include eucaryotic aggregates. Eucaryotes in general are less tolerant of D than bacteria.

Thus, in theory, neutron small angle scattering offers the biochemist the possibility of determining the relative location of the centers of scattering mass of subunits in macromolecular aggregates. Calculations made from experimental data obtained at the High Flux Beam Reactor (HFBR) at Brookhaven National Laboratory indicate that analysis of structures as large and complex as the bacterial ribosome is possible at the present time (22).

5 INSTRUMENTATION

5.1 *Objective*

The experimental objective is to collect scattering data of sufficient quality from biological specimens so that structural problems may be solved.

5.2 *The Problem*

A solution-scattering profile is a continuous function of scattering angle. In order to measure it perfectly, an infinitely fine beam of monochromatic neutrons must be directed at the specimen and the scattering distribution detected using a device with infinite spatial resolution (11). Obviously all these conditions must be relaxed

to make measurement possible. As the beam becomes larger, less well collimated, and less monochromatic, and as the detector resolution drops, the number of events per unit time measured at each angular position increases. The price paid is that the value obtained at each scattering angle instead of being proportional to $|\overline{F(\mathbf{R})}|^2$ becomes a weighted average of values of $|\overline{F(\mathbf{R})}|^2$ near that angle.

The divergence between the observed scattering profile and the measured values so produced can be corrected for in principle by data processing a posteriori. However, the mathematical manipulations required are deconvolutions, no matter what form the algorithm used may take (see below). Deconvolution of experimental data magnifies the influence of statistical error on the final result. Thus, while relaxation of geometric and chromatic stringency increases count rate at the detector, it also increases the requirement for more counts, that is, more statistical precision. There will clearly be a point in any experiment beyond which further relaxation degrades the data collected more than can be compensated for by the increase in counting rate. The issue then is to design the experiment to maximize the rate of information acquisition, not just the rate of data acquisition. The optimum in any situation will depend on the precision of the data required by the experiment. While the experience of those working with X-ray solution scattering in this area is of value as a guide to the design of neutron small angle experiments, there are some aspects of the neutron problem unique to it. These have to do mainly with the nature of neutron sources.

5.3 *The Neutron Source*

Neutrons are produced at fluxes appropriate for work of this type by uranium fission in the cores of nuclear reactors. These high energy neutrons pass from the core into a jacket of moderating material that surrounds it. In this region the neutrons lose energy by inelastic scattering, and eventually reach approximate thermal equilibrium with the moderating substance. Thus the kinetic energy distribution of neutrons in this region of the reactor approximates the Maxwell-Boltzmann spectrum appropriate for the temperature of the moderator. At the Brookhaven HFBR, for example, the moderator is D_2O maintained at 300K and the peak energy corresponds to a wavelength of 1 Å. By using a low temperature moderator (e.g. liquid H_2) the wavelength at maximum flux can be shifted to larger values (~ 6 Å). Since increasing the wavelength of the radiation used in a small angle experiment relaxes angular resolution restrictions, cold sources are highly desirable for such work. Installations of this type are in operation in at least two reactors (Julich and Grenoble); one will be available at Brookhaven in 1975.

A neutron-transparent window in the shielding that surrounds the moderator vessel constitutes the source. This window can be centimeters in diameter, providing a very large beam, a novel feature for those used to working with X-ray generators. The beam will supply neutrons with the same distribution of energies as found in the moderator. The flux of the source, however, is very low by X-ray standards. If one compares X-ray and neutron fluxes, X-ray sources are 10^7 times brighter for comparable wavelength bandwidths (see 4). Since neutron and X-ray cross sections are comparable in magnitude for macromolecules, the flux difference means that the scattered signal produced per weight of specimen per unit time is corre-

spondingly low in neutron experiments. For this reason, maximization of the rate of data acquisition is a major consideration in experimental design.

5.4 Apparatus Design

Once the angular resolution requirements of an experiment have been decided upon, one then can proceed to design an apparatus that yields data of the required precision at an optimal rate. Given the low flux available, an obvious way to obtain a decent data acquisition rate is to use large samples and irradiate these with beams having large cross-sectional areas. A typical specimen for a neutron low angle experiment contains tens of milligrams of material and is illuminated with a neutron beam one centimeter or more in diameter. Given the beam size, the beam must be well collimated and the detector distant from the specimen in order to maintain good angular resolution. Thus there is a marked tendency to hypertrophy in neutron small angle apparatus. The Grenoble small angle instrument is 80 m in length! There are obvious limitations on instrument size, however, set by constraints such as the availability and nature of sample material and the space available on the working floor of the facility being used. The trade-offs in profile accuracy involved in adjusting critical instrumental parameters such as beam size and chromatic width have been discussed recently by Schmatz et al (3). Ibel et al (27) have pointed out that optimum use of the available beam is made if an experiment is arranged so that each of the resolution limiting features in its design contributes equally to the deviation of the experimental curve from the ideal.

5.5 Current Instrumentation

Two basic kinds of apparatus are in use at present. The paired Soller slit spectrometer (28, 29) consists of a parallel array of collimating vanes in a rectangular support and a similar set of vanes at the detector (Figure 1B). The detector is moved through a series of scattering angles and the scattering curve is measured one point at a time. The arrangement is equivalent geometrically to the low angle X-ray apparatus in which two collimating slits define the beam and two detector slits are used to limit the measured scattering angles (30), except that the experiment is repeated many times in parallel by the array of apertures. Neutrons are reflected into the detector by a pyrolytic graphite crystal after the detector slits. The orientation of the graphite crystal controls the wavelength used in the experiment. This arrangement, as set up at Brookhaven, gives a well-defined beam (see Figure 2) that permits accurate measurement of scattering curves starting at $(600 \text{ \AA})^{-1}$ using 4 \AA neutrons. Its advantages are that good collimation and hence angular resolution can be obtained in an apparatus that is physically quite small (a few meters from beam source to detector) and yet makes good use of a large beam area. It is relatively cheap to build, and provided attention is paid to the construction of the vanes, cross talk between slits is surprisingly small. The principal disadvantage of the Soller slit spectrometer is that it is capable of measuring only one scattering angle at a time, an important limitation given the constraint of low neutron flux.

To our knowledge, a second type of apparatus is now in use at several

locations: Julich (31), Grenoble (3), and Brookhaven. The idea is to construct an instrument using detectors that record the scattering at many angles simultaneously instead of just one. The arrangement for such an experiment consists of a series of collimating apertures that define the beam impinging on the specimen and a detector (or detectors) positioned to collect a region of the scattering pattern (Figure 1A). Provided collimation is good and the sample to detector distance long, the full area of the available source can be used. The wavelength band to be measured must in this case be selected prior to collimation (not a requirement for the Soller slit spectrometer). Recent technological developments have produced position-sensitive neutron detectors that are capable of high spatial resolution and high efficiency (32). For example, the detector at the Brookhaven HFBR can detect 4 Å neutrons at 8000 locations over an 18 × 18 cm surface with more than 90% efficiency (33). Comparative measurements made with the position sensitive detector and Soller slit spectrometer show that gains of more than 100 in the rate of data acquisition are obtained from some specimens, as expected. Thus the

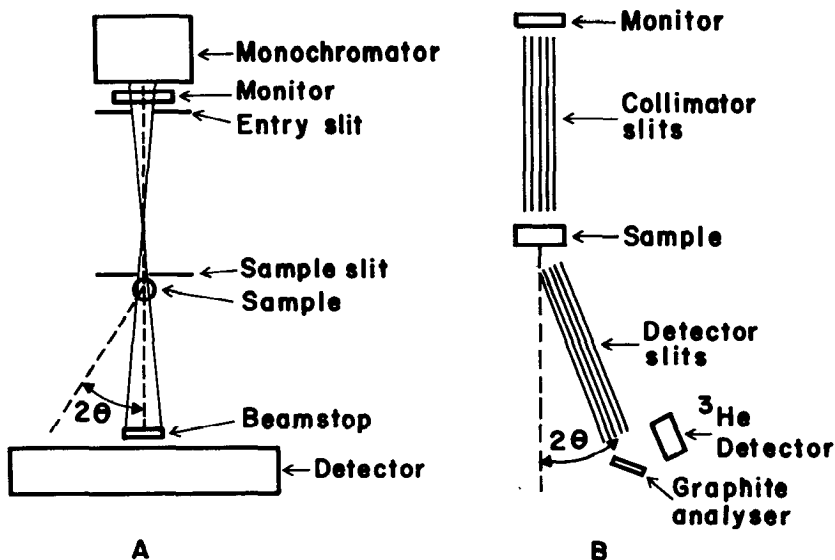


Figure 1 Neutron scattering apparatus. The two principal geometries now in use for neutron small angle scattering measurements are shown. A slit-collimated neutron source used after monochromatization of the beam is shown in (A). The neutrons pass through a monitor of the beam that allows the regulation of counting with respect to flux through the specimen. After the collimator, the neutrons scattered by the specimen are counted by a position-sensitive detector. A beamstop is used to prevent the main beam from reaching the detector. The Soller slit apparatus is shown in (B). The main differences are that an analyzer slit is used, monochromatization is accomplished after the scattering event by the graphite analyzer, and only one scattering angle is measured at a time.

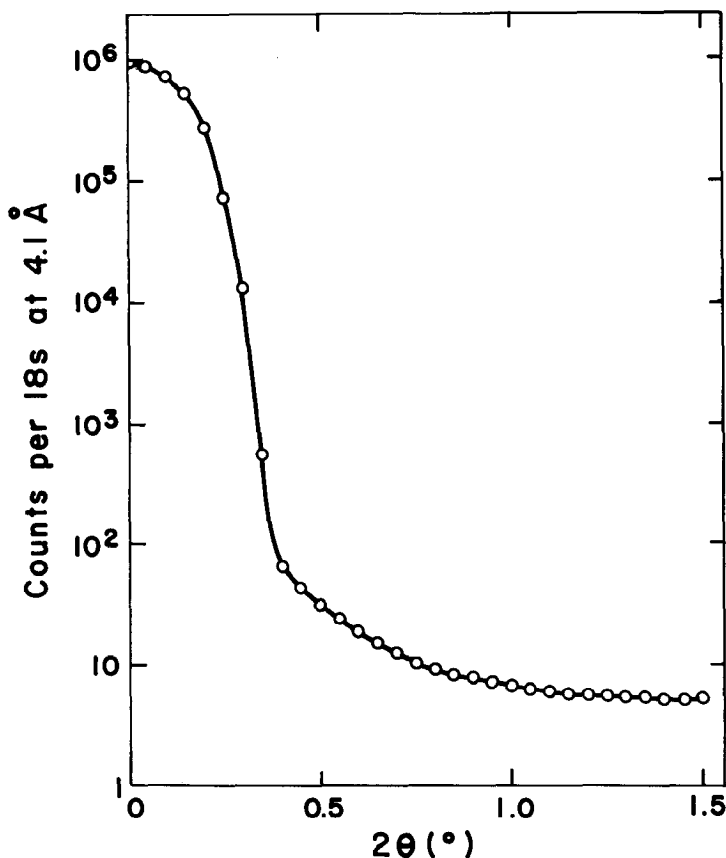


Figure 2 The beam profile as measured by the Soller slit apparatus is shown. The number of 4 Å neutrons measured at $\Delta\lambda/\lambda = 0.025$ per 10^5 monitor counts (about 18 sec) is shown as a function of 2θ . Actual counting times were larger for angles greater than 0.35° . A moderate amount of scattering from the vanes is seen from 0.4° – 1.0° , which contributes to background in a typical radius of gyration measurement.

instrument of choice at present for small angle work appears to be the collimator-position sensitive detector combination. It is worth emphasizing that reactors with fluxes smaller than those of Grenoble or Brookhaven can be used for the collection of useful biological data provided instrumentation of this type is used.

5.6 Wavelength Bandwidth

The continuous spectrum of neutron wavelengths provided by the reactor allows the experimentalist to choose the wavelength, λ , and wavelength band spread, $\Delta\lambda$, used in a given experiment. As with the geometric factors of a collimation

system, the degradation of the scattering curve by band spread should be comparable in magnitude to other factors at the largest angle of measurement, in order to optimize data acquisition rate. A typical value of $\Delta\lambda/\lambda$ for the Soller slit spectrometer is 0.025, where the wavelength bandwidth is mainly determined by the mosaic spread of the graphite monochromator crystal. This value is about two orders of magnitude larger than that for the Cu K α radiation commonly used in X-ray experiments, offsetting part of the relative flux disadvantage of neutron experiments. For some low angle scattering experiments, a $\Delta\lambda/\lambda > 0.1$ may be appropriate, with consequent gains of data acquisition rate (27).

There are three methods currently in use for selecting a band of neutron wavelengths from the reactor spectrum: filters, graphite crystals, and velocity selectors. Filters remove all wavelengths in the neutron spectrum less than a given value by multiple Bragg reflection in the filter material (4). Beryllium filters, for example, are commonly used to remove all radiation less than 4 Å from neutron beams. Pyrolytic graphite crystals reflect neutrons from the 002 planes of their lattice with high efficiency (34). The wavelength obtained depends on the orientation of the crystal to the incident neutron beam; the bandwidth is determined by the mosaic spread of the crystal. At present the largest mosaic crystals give $\Delta\lambda/\lambda \sim 0.025$, which is narrower than the optimum for many experiments. Other crystals have been used in the past for monochromation, but graphite is the best found so far for general use. A velocity selector is a rotating drum with helically arranged slots on its periphery. The drum axis is oriented parallel to the neutron beam and positioned so the slots intercept it. The velocity of the neutrons that get past the drum and hence their wavelength depends on its speed of rotation (35). Velocity selectors can produce wide band spreads ($\Delta\lambda/\lambda \sim 0.1$), but with the loss of a substantial portion of the available reactor flux at the wavelength in question. Of these methods, none is ideally suited to the low angle scattering measurements; however, a new technical development promises an improvement in this area. If alternate layers of material of different scattering length are deposited on a smooth surface such that the layers are of equal thickness, an efficient reflecting monochromator is produced in which $\Delta\lambda$ may be controlled by the number of layers deposited. Such multilayer monochromators have been produced at Brookhaven (36) and tests show them to have high reflectivity (>60%). In the future it may be possible to make curved multilayers which can be used as focusing mirrors, allowing one to make a neutron low angle spectrometer analogous to the Franks X-ray camera (37).

5.7 Data Processing

The use of finite beams and detectors as well as polychromatic radiation results in degradation of the measured scattering profile, as mentioned above. The purpose of data processing is to remove the contributions caused by lack of perfect geometry and perfect monochromatization. The problem of correcting scattering data for geometric aberration or "slit smearing" is common to both the X-ray and neutron small angle fields. The effects of slit smearing on data precision are well understood. A plethora of approaches to correcting data for these effects has been suggested e.g. (38–40).

Correction for chromatic effects, however, is a problem unique to the neutron

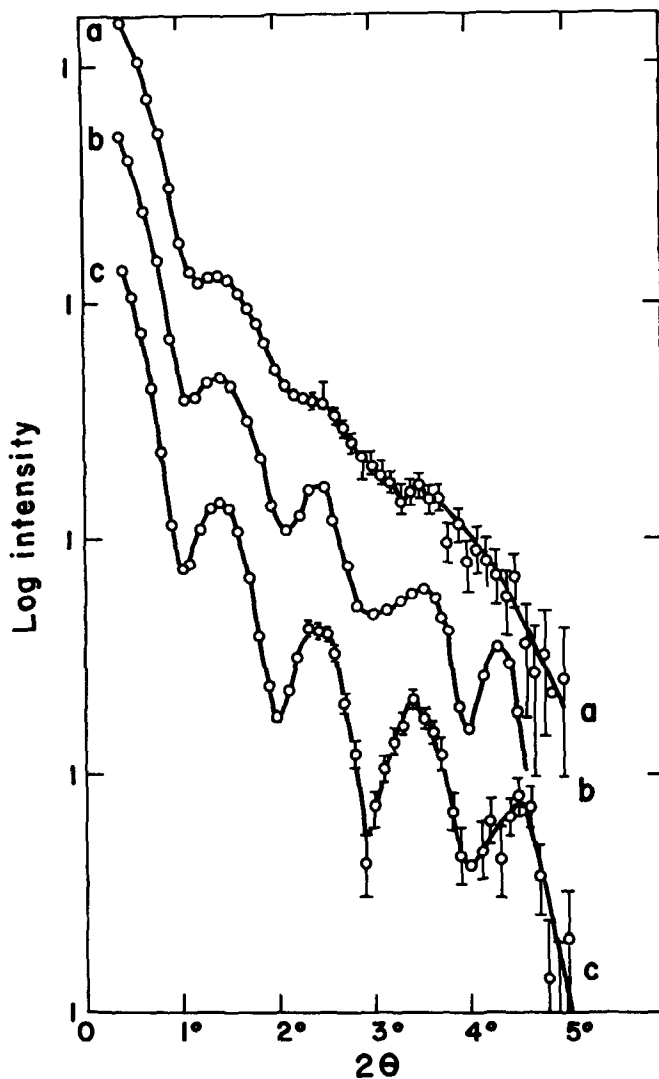


Figure 3 Three scattering curves of R17 bacteriophage are shown. The data were collected using the Soller slit apparatus at Brookhaven and a specimen of R17 phage kindly provided by Dr. Joan Argetsinger-Steitz. Curve *a* is the scattering profile measured in 2.5 h using the D₂O moderated reactor spectrum and a Be filter cooled with liquid N₂. λ max was 4.1 Å and $\Delta\lambda/\lambda \sim 0.1$. The wavelength profile was determined using the 002 reflection from a narrow mosaic graphite crystal. Curve *b* was obtained using the spline function procedure (39) to deconvolute the known wavelength profile from the observed scattering curve (curve *a*). Curve *c* was measured using a graphite analyzer crystal which gave λ max = 4.13 Å and $\Delta\lambda/\lambda = 0.025$. The data were obtained in 7.5 h. The three curves are arbitrarily scaled for purposes of comparison.

field. To illustrate the problem we show two scattering profiles collected on R17 bacteriophage using the Soller slit spectrometer at Brookhaven. In Figure 3c is shown the profile obtained in $7\frac{1}{2}$ h using a graphite monochromator with $\Delta\lambda/\lambda = 0.025$. Figure 3a is a profile collected in $2\frac{1}{2}$ h on the same specimen under identical conditions except that only a beryllium band pass filter was used for monochromatization ($\Delta\lambda/\lambda \sim 0.1$). A threefold gain in counting rate was achieved, but at the expense of losing much of the regular peak and valley structure characteristic of the phage scattering profile. A feature of chromatic smearing visible in Figure 3a is that its impact increases with scattering angle unlike geometric smearing. An attempt was made to correct these data for chromatic aberration using the generalized spline algorithm of Schelten & Hossfeld (39) (Figure 3b). While correction obviously improves the profile (i.e. brings it closer to that shown in Figure 3c), it does not restore the detail present in the data collected at $\Delta\lambda/\lambda = 0.025$. Clearly, in this case, it is doubtful that a gain in information acquisition rate was obtained by going to a broader wavelength band spread.

Our experience with correction procedures has led us to several conclusions concerning their application. First, as mentioned above, high data precision is essential for successful deconvolution of a badly smeared profile. When this fact is taken into account much of the advantage in counting rate obtained by collecting "bad" data is lost. Second, almost all correction procedures treat the recovery of secondary maxima in smeared sphere scattering functions such as that of R17 very well. Their accuracy in correcting the Guinier region, however, is often much less convincing. Accordingly it is our feeling that correction procedures should not be relied upon as a substitute for adequate angular resolution data collection. Scattering experiments should be designed to balance a minimum of data correction with reasonable data acquisition rates.

6 CURRENT STATUS OF BIOLOGICAL STUDIES

In this section we discuss the progress that has been made in the study of biological structures using low angle neutron scattering in solution. The reader will easily ascertain that results that advance our understanding of biological structures are few at this time, but that the early indications are that considerable progress may be expected in the next few years. We divide the areas into studies of unlabeled macromolecules in solution, and studies of structures that have been isotopically labeled.

6.1 *Unlabeled Macromolecules in Solution*

The pioneering efforts of groups at Julich and more recently Grenoble have led to the initial experimental studies confirming the applicability of low angle solution-scattering theory to studies on macromolecules using neutrons. The thrust of their experiments is in areas that involve measurements of the value of the scattering curve at zero angle, the radius of gyration, and the shape of extended scattering curves for macromolecules in solution.

6.1.1 ZERO ANGLE SCATTERING The forward scatter of a sample, $I(0)$, can be obtained by extrapolation of low angle profiles to $2\theta = 0$ using equation 5. From

measurements of $I(O)$ one can obtain information concerning the volume of a molecule, the dynamics of its H-D exchange, and in certain cases, the homogeneity of preparations.

If the atomic composition of a molecule is known, its molecular volume may be obtained by a contrast matching experiment. The scattering density of the solvent is varied by adjusting its H:D ratio and the forward scattering of the sample measured. From equation 4 one expects a plot of $I(O)^{1/2}$ vs ρ_{sol} to give a straight line. When the solvent mixture is such that $\rho = \rho_{\text{sol}}$ the forward scatter of the molecules vanishes. Knowing the solvent composition, ρ_{sol} can be calculated and the molecular volume found:

$$V = \frac{\rho_{\text{sol}}}{\sum_i b_i}$$

(see equation 3). Obviously the number of exchangeable hydrogens in the structure must be known to obtain an exact value. In their studies on hemoglobin, Schelten et al (41) calculated a volume of $84,000 \pm 2000 \text{ \AA}^3$ for the molecule from neutron data, in excellent agreement with the crystallographic value of $83,000 \text{ \AA}^3$ (42). The volume obtained in this way is that of the nonhydrated molecule, in contrast with the volume obtained hydrodynamically. In conjunction with other techniques such volume measurements could be useful in studies on hydration and volume change in macromolecules.

If the H:D ratio of the medium surrounding a protein molecule is changed rapidly the ensuing equilibration of the exchangeable H sites on the molecule can be followed as changes in the forward neutron scattering. At time zero, the exchangeable sites will have an H:D ratio like that of the medium surrounding the protein, prior to mixing, and, as a function of time, the H:D ratio will decay to that of the solvent after mixing. This is seen as a decrease in I_0 with time. Since measurements of I_0 may be rapid under favorable conditions, a time resolution vastly superior to that previously obtainable in exchange studies is made possible by the neutron scattering method (41). Recently Stuhmann (18) has reported exchange experiments on myoglobin where exchange at 1 sec after mixing was measured and an initial decay with a time constant of 1.8 sec was successfully followed. It is projected (18) that a time resolution of 0.1 sec can be realized using the present scattering apparatus at Grenoble. Stuhmann points out that an interesting extension of these measurements can be obtained by following the time course of the change of other parameters of the scattering curve after a solvent shift, e.g. the radius of gyration of the macromolecule. Under these circumstances the dynamics of the radial distribution of exchanged sites may be accessible to measurement, and an improved understanding of diffusion in proteins should result (18).

The third application of forward scattering measurements concerns the special case of structures having regions that differ in ρ and may differ in the ratio of material in the different regions. Examples of such structures are the iron and protein in ferritin and the lipid and protein in serum lipoproteins. If preparations of such molecules are heterogeneous in the ratio of their contrasting components, there will be no solvent condition which gives a forward scatter of zero in a contrast

matching experiment. Analysis of contrast matching data for ferritin has shown that variations in the iron content lead to variations in the 600,000 mol wt of $\pm 200,000$ (18). The main limitation of the technique is that it requires precise data collection in situations where $(\rho - \rho_{\text{sol}})$ is small and the signal to be measured correspondingly low.

6.1.2 RADIUS OF GYRATION It has been shown (15, 16) that the radius of gyration observed for a macromolecule can be regarded as the sum of the radius of gyration of a homogeneous particle of the same external shape, R_f , and a second contribution that arises from internal scattering density fluctuations, where the contribution of internal features depends on the average contrast of the particle $(\rho - \rho_{\text{sol}})$:

$$R^2 = R_f^2 + \frac{B}{\rho - \rho_{\text{sol}}}. \quad 10.$$

The validity of this expression has been shown in a number of cases using X rays (16). The linearity of the dependence of observed radius of gyration on $(\rho - \rho_{\text{sol}})^{-1}$ also has been shown for a number of molecules including ferritin, low density serum lipoprotein, myoglobin, and lysozyme using neutron scattering (18). For most proteins, B is small and positive, consistent with the slightly H-rich center in these structures expected from the higher concentration of hydrophobic residues in this region. In the case of low density lipoprotein, the contrast is much larger and B is large and positive (18). Ferritin is an extraordinary case in which the presence of an iron core having high scattering density relative to protein produces a large negative value for B . For contrasts in which the average scattering density of the molecule is slightly above ρ_{sol} , R^2 becomes negative (see section 4.2).

Equation 10 can be derived from equation 7 if one assumes that the two contrasting regions in a structure have coincident centers of mass (i.e. $\Delta = 0$). It turns out that if Δ is not zero, a plot of R^2 vs $(\rho - \rho_{\text{sol}})^{-1}$ will be nonlinear. Thus, the observation that the data of ferritin, for example, fall on a straight line (18) indicates that the iron and protein mass distributions are concentric.

When molecules of low internal contrast are examined under conditions such that $(\rho - \rho_{\text{sol}})$ is large, the neutron radius of gyration of a molecule will be close to the X-ray value, which in turn will correspond reasonably well to the mechanical radius of gyration of the molecule. [See (45) and (41) for a demonstration of this fact for hemoglobin.]

Measurement of the radius of gyration as a function of solvent contrast thus appears to be a promising method for the study of internal compositional fluctuations, particularly in cases where the fluctuations can be reasonably considered as concentric.

6.1.3 EXTENDED SCATTERING CURVES The concept of analyzing extended scattering profiles into their shape and internal contrast components has already been mentioned (Section 4.2). Results obtained by this means using neutron data have only just begun to appear (18). As an example of a problem that could be resolved in this way, we might mention an old controversy about the bacterial ribosome.

The extended X-ray scattering profile of ribosomes includes some noticeable "peaks" at moderate angle (46, 47). The problem is to decide whether these peaks are incidental features of the shape transform of the particle or reflect regularities in its internal structure. Both positions have had their exponents (48, 49). A properly designed neutron experiment could answer the question.

6.2 Studies on Specifically Labeled Macromolecules

As pointed out earlier, the scattering contrast within a macromolecular complex can be controlled by specific deuteration of its subunits. Deuteration can be used either to enhance preexisting contrasts or to create contrasts that do not normally exist. In either case, the objective of deuteration is to extend the range of possibilities available for investigating structures by contrast control methods. To date, to the best of our knowledge, only one such experiment has been reported in the literature, work involving the 50S ribosomal subunit from *E. coli* (50).

The ribosomal subunits of *E. coli* are complexes of RNA and protein. Because of the difference in the biochemical pathways that lead to RNA and protein synthesis, it is easy to devise growth conditions that result in preferential incorporation of D into the protein portion of these particles. Particles grown under three different growth conditions were isolated and suspended in solvents whose H:D ratios were chosen to give distinctive and different relative scattering lengths for RNA and protein in each sample. Radii of gyration were measured in all three specimens. The scattering lengths for protein and RNA in each specimen were determined so that weighting factors (see equation 7) could be obtained. The results are given in Table 3, along with the data obtained from similar experiments on the 30S

Table 3 Radius of gyration values for the ribosomal subunits of *E. coli*

Parameter ^a	Subunit	
	30S ^b	50S ^c
R_{RNA}	$67.2 \pm 2.2 \text{ \AA}$	$72.5 \pm 1.5 \text{ \AA}$
R_{protein}	$73.7 \pm 1.2 \text{ \AA}$	$73.4 \pm 2.0 \text{ \AA}$
$R_{\text{total structure}}$	$71.4 \pm 0.6 \text{ \AA}$	$78.0 \pm 1.0 \text{ \AA}$
$\Delta_{\text{RNA-protein}}$	$17.1 \begin{matrix} + 9.0 \\ - 19.0 \end{matrix} \text{ \AA}$	$57.5 \pm 10 \text{ \AA}$

^a R_{RNA} and R_{protein} are the radii of gyration of the RNA and protein portion of the subunit in question. $R_{\text{total structure}}$ is the radius of gyration of the subunit fully H substituted in a 100% D₂O solvent. Δ is the distance between the centers of mass of the RNA and protein distributions in the whole structure.

^b Moore, Engelman & Schoenborn, unpublished results.

^c See Ref. 50.

ribosomal subunit (Moore, Engelman & Schoenborn, unpublished results). The most interesting finding to emerge is that the 50S subunit is asymmetric in its distribution of RNA and protein. The centers of mass of the RNA and protein distributions are separated by about 58 Å, a large value compared to the maximum dimension of the particle, 230 Å (47). This result could not have been anticipated from earlier data and is one of the first novel findings to emerge from neutron low angle studies.

7 CONCLUSION

It is clear that the analysis of quaternary structure by neutron scattering has just begun. Solutions to the instrumentation problems and theoretical issues that occupied everybody's time over the last five to ten years have reached a satisfactory state, so that further progress will increasingly depend on the biochemical community. The ultimate success or failure of the field will depend on whether or not it provides us with biologically significant results about important macromolecular structures. This will happen if biochemists decide to make use of this new tool, and make the effort necessary to prepare suitable specimens. It is our expectation that interesting biological data will begin to emerge over the next few years.

ACKNOWLEDGMENTS

We wish to thank Dr. Benno P. Schoenborn for his advice and help. This work was supported by a grant from the National Science Foundation (NSF-GB-39275X). Neutron data were collected using the High Flux Beam Reactor at Brookhaven National Laboratory under the auspices of the Atomic Energy Commission.

Literature Cited

1. Schoenborn, B. P., Nunes, A. C. 1972. *Ann. Rev. Biophys. Bioeng.* 1:529-52
2. Schoenborn, B. P., Nunes, A. C., Nathans, R. 1970. *Ber. Bunsenges.* 74:1202-7; Schoenborn, B. P. 1975. In *Harwell Symp. Neutron Diffr.*, ed. R. D. Lowde. Fair Lawn, N. J.: Oxford Univ. Press. In press
3. Schmatz, W., Springer, T., Schelten, J., Ibel, K. 1974. *J. Appl. Cryst.* 7:96-116
4. Bacon, G. E. 1962. *Neutron Diffraction*. London: Oxford Univ. Press
5. Marshall, W., Lovesey, S. W. 1971. *The Theory of Thermal Neutron Scattering*. London: Oxford Univ. Press
6. See Ref. 5, Chap. 1
7. Shull, C. G. 1962. *International Tables for X-ray Crystallography*, ed. C. H. MacGillavry, G. D. Rieck, K. Lonsdale, Vol. III, pp. 197, 229. Birmingham, England: Kynoch. See also Ref. 1, 544-45
8. Schoenborn, B. P. 1971. *Cold Spring Harbor Symp. Quant. Biol.* 36:569-75
9. James, R. W. 1948. *The Optical Principles of the Diffraction of X-rays*. London: G. Bell
10. Guinier, A. 1963. *X-ray Diffraction*. San Francisco: Freeman
11. Guinier, A., Fournet, G. 1955. *Small Angle Scattering of X-rays*. New York: Wiley
12. Kratky, O., Pilz, I. 1972. *Quart. Rev. Biophys.* 5:481-537
13. Guinier, A. 1939. *Ann. Phys.* 12:161-237
14. Beeman, W. W., Kaesberg, P., Anderegg, J. W., Webb, M. B. 1957. *Handb. Phys.* 32:321-442
15. Kirste, R. G., Stuhmann, H. B. 1967. *Z. Phys. Chem. N.F.* 56:338-41
16. Stuhmann, H. B., Kirste, R. G. 1967. *Z. Phys. Chem. N.F.* 56:334-37
17. Stuhmann, H. B. 1973. *J. Mol. Biol.*

- 77:363-69
18. Stuhmann, H. B. 1974. *J. Appl. Cryst.* 7:173-78
19. Goldstein, H. 1959. *Classical Mechanics*. Reading, Mass.: Addison-Wesley
20. Damaschun, G., Fichtner, P., Purschel, H.-V., Reich, J. G. 1968. *Acta Biol. Med. Germ.* 21:309-16
21. Hoppe, W. 1972. *Isr. J. Chem.* 10:321-33
22. Engelman, D. M., Moore, P. B. 1972. *Proc. Nat. Acad. Sci. USA* 69:1997-99
23. Debye, P. 1915. *Ann. Phys.* 46:809-23
24. Kratky, O., Worthmann, W. 1947. *Monatsch. Chem.* 76:263-81
25. Hoppe, W. 1973. *J. Mol. Biol.* 78:581-85
26. DeRosier, D. J., Oliver, R. M. 1971. *Cold Spring Harbor Symp. Quant. Biol.* 36:199-203
27. Ibel, K., Schmatz, W., Springer, T. 1971. *Atomkernenergie* 17:15-18
28. Nunes, A. C. 1973. *Nucl. Instrum. Methods* 108:189-91
29. Haywood, B. C. G., Worcester, D. L. 1973. *J. Phys. E: J. Sci. Instrum.* 6:568-71
30. Anderegg, J. W., Beeman, W. W., Shulman, S., Kaesberg, P. 1955. *J. Am. Chem. Soc.* 77:2927-37
31. Christ, J., Schilling, W., Schmatz, W., Springer, T. 1965. *Z. Angew. Phys.* 18:295-308
32. Borkowski, C. J., Kopp, M. K. 1968. *Rev. Sci. Instr.* 39:1515-22
33. Alberi, J., Fischer, J., Fadeka, V., Schoenborn, B. P. *Proc. IEEE*. Submitted for publication
34. Gould, R. W., Bates, S. R., Sparks, C. J. 1968. *Appl. Spectrosc.* 22:549-51; Graves, N. F., Moore, A. W., Strong, S. L. 1969. *Proc. Bienn. Conf. Carbon, 9th, Boston, Mass.*, pp. 20-21
35. Buras, B., Mikke, K., Lebeck, B., Leciejewicz, J. 1965. *Phys. Status Solidi* 11:567
36. Schoenborn, B. P., Caspar, D. L. D., Kammerer, O. 1975. *J. Appl. Cryst.* In press
37. Franks, A. 1958. *Brit. J. Appl. Phys.* 9:349-52
38. Hossfeld, F. 1968. *Acta Cryst. A* 24:643-50
39. Schelten, J., Hossfeld, F. 1971. *J. Appl. Cryst.* 4:210-22
40. Glatter, O. 1974. *J. Appl. Cryst.* 7:147-53
41. Schelten, J., Schlecht, P., Schmatz, W., Mayer, A. 1972. *J. Biol. Chem.* 247:5436-41
42. Bragg, S. L., Howells, E. R., Perutz, M. F. 1954. *Proc. Roy. Soc. A* 222:33-44
43. Hvidt, A., Nielsen, S. O. 1966. *Advan. Protein Chem.* 21:288-386
44. Mateu, L., Tardieu, A., Lazzati, V., Aggerbeck, L., Scanu, A. M. 1972. *J. Mol. Biol.* 70:105-15
45. Conrad, H., Mayer, A., Schwaiger, S., Schneider, R. 1969. *Z. Physiol. Chem.* 350:845-50
46. Zubay, G., Wilkins, M. H. F. 1960. *J. Mol. Biol.* 2:105-12; Klug, A., Holmes, K. C., Finch, J. T. 1961. *J. Mol. Biol.* 3:87-100; Langridge, R., Holmes, K. C. 1962. *J. Mol. Biol.* 5:611-17
47. Hill, W. E., Thompson, J. D., Anderegg, J. W. 1969. *J. Mol. Biol.* 44:89-102
48. Van Holde, K. E., Hill, W. E. 1974. To appear in *The Ribosomes*, Cold Spring Harbor Lab., Cold Spring Harbor, NY
49. Venable, J. H. Jr., Spencer, M., Ward, E. 1970. *Biochim. Biophys. Acta* 209:493-500
50. Moore, P. B., Engelman, D. M., Schoenborn, B. P. 1974. *Proc. Nat. Acad. Sci. USA* 71:172-76

CONTENTS

EEG ANALYSIS: A HISTORY AND A PROSPECTUS, <i>Harold W. Shipton</i>	1
COMPUTER METHODS IN ELECTROCARDIOGRAPHY, <i>Hubert V. Pipberger, Rosalie A. Dunn, and Alan S. Berson</i>	15
THEORY, MEASUREMENT, AND APPLICATION OF THERMAL PROPERTIES OF BIOMATERIALS, <i>H. Frederick Bowman, Ernest G. Cravalho, and Monty Woods</i>	43
ON THE EVOLUTION OF THE PHYSIOLOGICAL MODEL, <i>William S. Yamamoto and Ellen S. Walton</i>	81
COMPUTER-AIDED INSTRUCTION IN MEDICINE, <i>Edward P. Hoffer, G. Octo Barnett, Barbara B. Farquhar, and Penny A. Prather</i>	103
CHEMOTAXIS IN BACTERIA, <i>Howard C. Berg</i>	119
MUSCLE FILAMENT STRUCTURE AND MUSCLE CONTRACTION, <i>J. M. Squire</i>	137
ELECTRON MICROSPECTROSCOPY, <i>M. S. Isaacson and A. V. Crewe</i>	165
THE EMERGENCE AND REGULATION OF SPATIAL ORGANIZATION IN EARLY ANIMAL DEVELOPMENT, <i>J. Cooke</i>	185
DETERMINATION OF QUATERNARY STRUCTURE BY SMALL ANGLE NEUTRON SCATTERING, <i>D. M. Engelman and P. B. Moore</i>	219
THE APPLICATION OF INTENSITY FLUCTUATION SPECTROSCOPY TO MOLECULAR BIOLOGY, <i>Francis D. Carlson</i>	243
THE PHYSICAL STATE OF DIFFUSIBLE IONS IN CELLS, <i>Hommo T. Edzes and Herman J. C. Berendsen</i>	265
FLUORESCENT PROBES IN NERVE MEMBRANES, <i>F. Conti</i>	287
CONCENTRATION CORRELATION SPECTROSCOPY: A NEW BIOPHYSICAL PROBE BASED ON OCCUPATION NUMBER FLUCTUATIONS, <i>E. L. Elson and W. W. Webb</i>	311
ANTIBIOTICS AND MEMBRANE BIOLOGY, <i>Stuart McLaughlin and Moisés Eisenberg</i>	335
BIOMEDICAL MATERIALS, <i>Donald F. Gibbons</i>	367

CALCIUM TRANSPORT IN SARCOPLASMIC RETICULUM, <i>David H. MacLennan and Paul C. Holland</i>	377
ARTIFICIAL KIDNEYS: PROBLEMS AND APPROACHES, <i>C. F. Gutch</i>	405
SURVIVAL DISTRIBUTION, <i>Virginia A. Clark</i>	431
COMPUTER MONITORING IN PATIENT CARE, <i>Donald H. Glaeser and Lewis J. Thomas Jr.</i>	449
AN ANALYSIS OF THE STRUCTURE OF tRNA, <i>Paul B. Sigler</i>	477
COMPUTERS IN THE CLINICAL PATHOLOGIC LABORATORY : CHEMISTRY AND IMAGE PROCESSING, <i>Lewis E. Lipkin and Bernice Sacks Lipkin</i>	529
INDEXES	
AUTHOR INDEX	579
CUMULATIVE INDEX OF CONTRIBUTING AUTHORS, VOLUMES 1-4	601
CUMULATIVE INDEX OF CHAPTER TITLES, VOLUMES 1-4	602